ROYAL SOCIETY OPEN SCIENCE

rsos.royalsocietypublishing.org

Research

**Cite this article:** Xu Q, Yang W, Cui S, Street J, Luo Y. 2018 Sulfur resistance of Ce-Mn/$TiO_2$ catalysts for low-temperature $NH_3$–SCR. *R. Soc. open sci.* **5**: 171846.
http://dx.doi.org/10.1098/rsos.171846

Received: 8 November 2017
Accepted: 5 February 2018

**Subject Category:**
Chemistry

**Subject Areas:**
materials science

**Keywords:**
$NH_3$–SCR, sulfur resistance, Ce-Mn/$TiO_2$ catalyst, catalyst synthesis

**Author for correspondence:**
Quan Xu
e-mail: xuquan@cup.edu.cn

This article has been edited by the Royal Society of Chemistry, including the commissioning, peer review process and editorial aspects up to the point of acceptance.

THE ROYAL SOCIETY PUBLISHING

# Sulfur resistance of Ce-Mn/$TiO_2$ catalysts for low-temperature $NH_3$–SCR

Quan Xu[1], Wenjing Yang[1], Shitong Cui[1], Jason Street[2] and Yan Luo[3]

[1]State Key Laboratory of Heavy Oil Processing, Institute of New Energy, China University of Petroleum, Beijing 102249, People's Republic of China
[2]Department of Sustainable Bioproducts, Mississippi State University, Mississippi, MS 39762, USA
[3]Department of Chemical Engineering, West Virginia University, Morgantown, WV 26505, USA

QX, 0000-0003-2195-2513

Ce-Mn/$TiO_2$ catalyst prepared using a simple impregnation method demonstrated a better low-temperature selective catalytic reduction of NO with $NH_3$ ($NH_3$–SCR) activity in comparison with the sol-gel method. The Ce-Mn/$TiO_2$ catalyst loading with 20% Ce had the best low-temperature activity and achieved a NO conversion rate higher than 90% at 140–260°C with a 99.7% NO conversion rate at 180°C. The Ce-Mn/$TiO_2$ catalyst only had a 6% NO conversion rate decrease after 100 ppm of $SO_2$ was added to the stream. When $SO_2$ was removed from the stream, the catalyst was able to recover completely. The crystal structure, morphology, textural properties and valence state of the metals involving the novel catalysts were investigated using X-ray diffraction, $N_2$ adsorption and desorption analysis, X-ray photoelectron spectroscopy, scanning electron microscopy and energy dispersive spectroscopy, respectively. The decrease of $NH_3$–SCR performance in the presence of 100 ppm $SO_2$ was due to the decrease of the surface area, change of the pore structure, the decrease of $Ce^{4+}$ and $Mn^{4+}$ concentration and the formation of the sulfur phase chemicals which blocked the active sites and changed the valence status of the elements.

## 1. Introduction

Nitrogen oxides $NO_x$ (NO, $NO_2$, $N_2O$) are global by-products of high-temperature combustion [1]. $NO_x$ abatement from emissions is necessary because emitted nitrogen oxides cause severe adverse health effects, acid rain and ozone layer depletion [2–6]. Among the $NO_x$ treatment approaches, the technology involving the selective catalytic reduction (SCR) of $NO_x$ with $NH_3$ ($NH_3$–SCR) has been regarded as the most effective and widely

used method because of its high denitration efficiency and wide operable temperature range [7]. The SCR method refers to the process in which the reducing agent $NH_3$ reacts with $NO_x$ with the assistance of catalyst, generating $N_2$ and $H_2O$ [8]. The reactions involved in this process can be seen in the following equations

$$4NH_3 + 4NO + O_2 \rightarrow 4N_2 + 6H_2O, \tag{1.1}$$

$$4NH_3 + 2NO_2 + O_2 \rightarrow 3N_2 + 6H_2O, \tag{1.2}$$

$$4NH_3 + 3O_2 \rightarrow 2N_2 + 6H_2O, \tag{1.3}$$

$$2NH_3 + 2O_2 \rightarrow N_2O + 3H_2O \tag{1.4}$$

and

$$2NH_3 + 2NO_2 + 2NO \rightarrow 2N_2 + 3H_2O. \tag{1.5}$$

Reactions (1.1) and (1.2) are designated as the main reactions, and reaction (1.1) is often regarded as the standard SCR reaction. Elevated temperature may lead to the occurrence of $NH_3$ oxidation side effects, partly shown in equations (1.3) and (1.4). The coexistence of $NH_3$, NO and $NO_2$ will lead to a rapid SCR reaction, shown in equation (1.5). Studies have shown that the reaction rate of equation (1.5) is faster than that of standard SCR reactions.

The fundamental goal of $NH_3$–SCR technology is to develop a SCR catalyst that possesses a high activity at relatively low temperature ranges, strong anti-sulfur performance and vanadium-free to be environmentally friendly. Metal oxide catalyst groups that are Mn-based [9–11] and Ce-based [12–14] have high efficiencies at low temperature ranges because of the reduction of $Mn^{4+}$ to $Mn^{3+}$ in the Mn phase, and $CeO_2$ has a considerably large oxygen storage capacity and excellent redox properties. Composite catalysts prepared using these two kinds of active components have favourable low-temperature denitration activity and are stable when introduced to typical catalyst poisons. In addition, the vast surface area, developed pore structure and acid sites of $TiO_2$ are more conducive to the adsorption of $NH_3$ and can accelerate the reaction [15–17]. Qi *et al*. [18] prepared a non-load-type $MnO_x$-$CeO_2$, low-temperature SCR catalyst using co-precipitation. The removal of NO was boosted by improving the ability of the redox catalyst by infusing Mn in the $CeO_2$ lattice. This generated a large number of oxygen vacancies. Lee *et al*. [19] prepared a $MnO_x/CeO_2$-$TiO_2$ catalyst. They found that Ce doping increased the surface area of the catalyst, improved the $Mn^{4+}$ concentration and increased the overall catalytic activity. Liu *et al*. [3] proved that the environmentally benign Mn-Ce-Ti catalyst had a high affinity for $NO_x$ removal because of the dual redox properties and the amorphous structure of the catalyst. Moreover, the Mn-Ce-Ti catalyst displayed a high resistance towards $H_2O$ and $SO_2$.

The principal objective of this study involves determining how well the co-doped Ce-Mn/$TiO_2$ catalyst can tolerate sulfur while undergoing low-temperature SCR. A series of Ce-Mn/$TiO_2$ catalysts were prepared using a single impregnation (IP) method and investigated for their effectiveness of low-temperature SCR of $NO_x$ with $NH_3$. The possible mechanism of the best performing, low-temperature SCR catalyst in this work is discussed in detail using various characterization methods.

# 2. Material and methods

## 2.1. Catalyst preparation

Catalysts were prepared using previously discussed IP and sol-gel (SG) methods [20,21]. The IP method involved using a molar ratio of 2 : 3 manganese acetate to cerium nitrate. The components were dissolved in deionized water and stirred for 1 h. Subsequently, approximately 2.5 g of $TiO_2$ was added to the mixture and stirred for 2 h. The suspension was transferred to a rotary evaporator and heated at 55°C for 1 h to obtain the viscous liquid. This sample was dried at 105°C overnight in an oven. Subsequently, the sample was calcined at 550°C for 6 h and ground to a mesh size of 20–40. The mass ratio of Ce/$TiO_2$ was tuned and recorded as Ce(wt%)-Mn/$TiO_2$. The molar ratio of Mn and Ce element maintains constant in each catalyst.

The SG method involved using 2.65 g of tetra-n-butyl titanate and 21.2 g of ethanol. The components were mixed and stirred for 50 min to form a yellow-tinted solution referred to as 'solution A'. A separate solution of manganese nitrate and cerium nitrate was dissolved in deionized water, and then anhydrous ethanol and acetic acid were added. This solution was stirred for 1 h to obtain a red-tinted solution referred to as 'solution B'. Subsequently, solution B was slowly added to solution A, and the mixture was stirred for 12 h. The gel formed at a room temperature for 2 h. The gel was then dried at 105°C for 24 h and calcined at 500°C for 2 h in a 20% $O_2$ flow. The final sample was ground to a mesh size ranging from

20 to 40. The ratio of tetra-n-butyl titanate, ethanol, deionized water and acetic acid was 1 : 8 : 6 : 3. The molar ratio of manganese element and cerium was 2 : 3 (the same ratio used with the IP method outlined above).

## 2.2. Catalyst activity measurement

SCR activity of the catalyst was measured using a fixed bed, stainless steel tube reactor with an inner diameter of 11 mm and an outer diameter of 14 mm. Gas purchased to be used in the experiment contained specific concentrations of components to simulate flue gas. The feed gas mixture consisted of 500 ppm $NH_3$, 500 ppm NO, 3% $O_2$ (volume fraction), 0–200 ppm $SO_2$ (depending on the experiment) and a balance of $N_2$. The simulated gas flow rate was 1000 ml $min^{-1}$. A volume of 6 ml of catalyst was loaded into the reactor for each experiment. The temperature ranged 100°C and 300°C at a heating rate of 3°C/min with a gas hourly space velocity (GHSV) of 10 000 $h^{-1}$. The concentrations of NO were monitored at the inlet and outlet in real time using a gas analyser (Testo 340) to calculate the conversion rate using the following equation.

$$\text{NO conversion } (\%) = \frac{[\text{NO}]_{\text{in}} - [\text{NO}]_{\text{out}}}{[\text{NO}]_{\text{in}}} \times 100\%, \tag{2.1}$$

where $[\text{NO}]_{\text{in}}$ and $[\text{NO}]_{\text{out}}$ referred to the NO concentration at the reactor inlet and outlet, respectively. The concentration was measured when the reaction reached a steady-state condition (approx. 20–40 min) at each temperature, which reduced the measurement errors caused by instability.

## 2.3. Catalyst characterization

The powder X-ray diffraction (XRD) characterization of the samples was performed using a Bruker D8-Advance X-ray powder diffractometer with a Cu K$\alpha$ radiation source ($\lambda = 1.5406$ Å), a pulverized sample with scattering angles ($2\theta$) of 5–85° and a 0.0197 step size operated at 50 kV and 50 mA. The diffraction lines were identified by matching them with reference patterns in the Joint Committee on Powder Diffraction Standards (JCPDS) database.

A ThermoFisher Escalab 250Xi X-ray powder photoelectron spectrometer was used to qualitatively analyse the X-ray photoelectron spectroscopy (XPS) characterization of the sample surface composition using an Al K$\alpha$ radiation source with a scattering of 0–5000 eV. The binding energy was calibrated using the C 1s peak contaminate carbon (BE = 284.6 eV) as an internal standard.

$N_2$ adsorption and desorption of each sample were measured at −196°C using the ASAP 2020 automatic rapid surface area and mesoporous/microporous analyser with a $N_2$ adsorption gas. The samples were degassed at 200°C for 12 h before the measurement took place. The specific surface area was calculated according to the Brunauer–Emmett–Teller (BET) method. The total pore volume was determined based on the amount of the adsorbed $N_2$ volume at a relative pressure of approximately $p/p_0 = 0.99$.

The surface morphology of the catalysts was characterized with scanning electron microscopy (SEM) using a Hitachi SU8010 with an acceleration voltage of 15 kV. Qualitative and quantitative analysis of catalyst elements were carried out using energy dispersive X-ray spectroscopy (EDS) on a HORIBA EX-350 with an acceleration voltage of 15 KV.

# 3. Results

## 3.1. Effect of synthetic method on the $NH_3$–SCR activity

SCR activities of the Ce(20)-Mn/$TiO_2$ catalysts synthesized by the SG and IP methods are shown in figure 1. These results reveal that the IP method had a better low-temperature denitration activity than the SG method. At a temperature range of 140–260°C, the NO conversion rate was higher than 90% in the presence of the IP catalyst. At a temperature range of 160–300°C, the NO conversion rate was higher than 90% in the presence of the SG catalyst. The NO conversion rate was approximately 99.7% at a temperature of 180°C using either method. The catalyst made using the IP method showed better low-temperature denitration activity, was easy to prepare, and had a low-cost preparation process. Therefore, the following Ce-Mn/$TiO_2$ catalysts used in this study were prepared using the IP method.

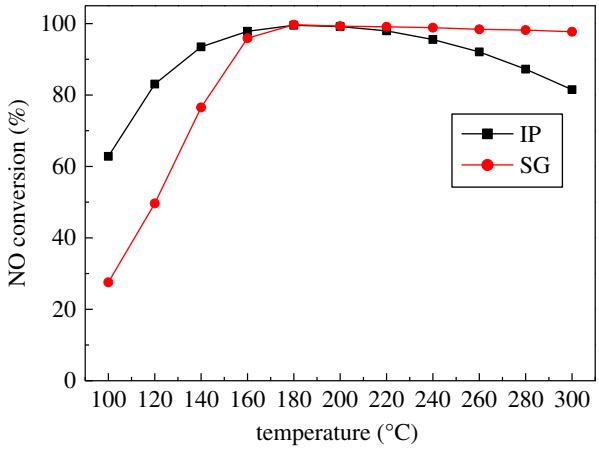


**Figure 1.** The influence of synthesis methods on $NH_3$–SCR activity. IP, impregnation method; SG, sol-gel method (500 ppm NO, 500 ppm $NH_3$, 3% $O_2$, $N_2$ balance gas, GHSV = 10 000 $h^{-1}$).

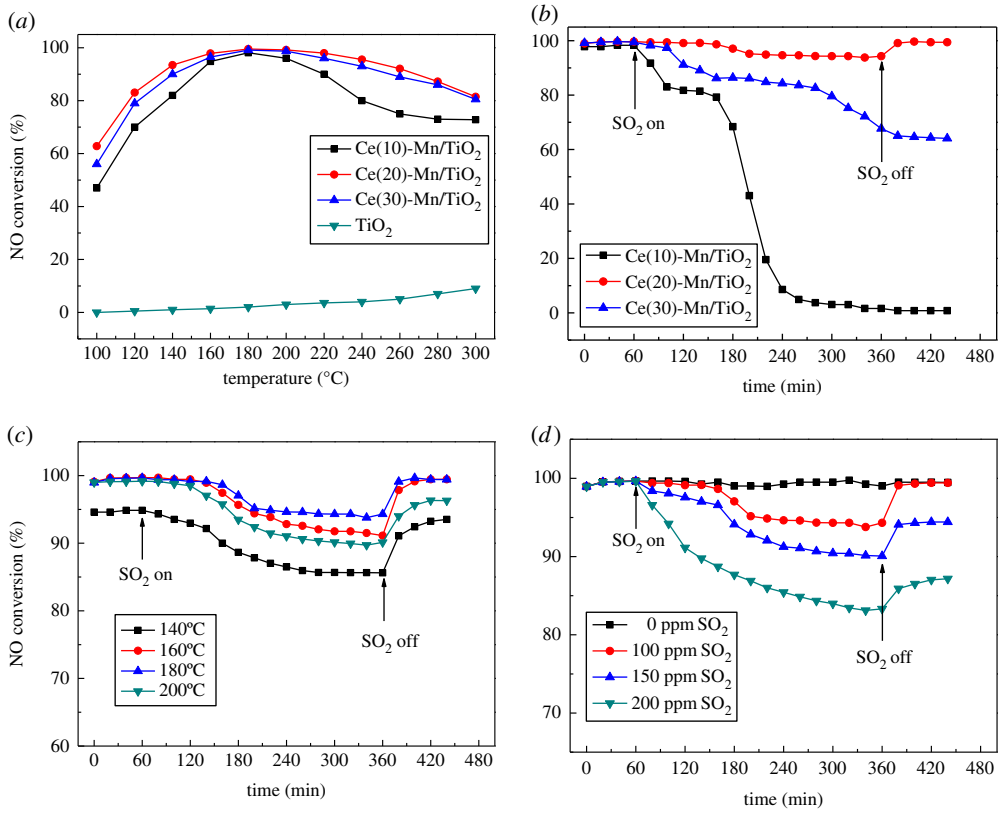


**Figure 2.** (*a*) Catalytic activity of Ce-Mn/$TiO_2$ catalyst for $NH_3$–SCR. Catalysts were loaded with 10%, 20% and 30% Ce and denoted as Ce(10), Ce(20) and Ce(30), respectively. Pure $TiO_2$ was also used for comparison. (*b*) The effect of various Ce concentrations using a Ce-Mn/$TiO_2$ catalyst on $SO_2$ resistance. (*c*) The effects of reaction temperature on NO conversion of the Ce(20)-Mn/$TiO_2$ catalyst in the presence of $SO_2$. The above three types of reactions were performed at: 500 ppm NO, 500 ppm $NH_3$, $SO_2$ 100 ppm, 3% $O_2$, $N_2$ balance gas, GHSV = 10 000 $h^{-1}$. (*d*) The effects of $SO_2$ concentration on NO conversion of Ce(20)-Mn/$TiO_2$ catalysts ($T$ = 180°C, 500 ppm NO, 500 ppm $NH_3$, 3% $O_2$, $N_2$ balance gas, GHSV = 10 000 $h^{-1}$).

## 3.2. Resistance to $SO_2$ poisoning on Ce-Mn/$TiO_2$ catalysts

The addition of active components has a crucial effect on the catalyst performance in $NH_3$–SCR. As shown in figure 2*a*, the $NO_x$ conversion rate on pure $TiO_2$ was less than 10% in the temperature range of 100–300°C, indicating that the carrier was inactive for denitration. After adding Ce and Mn, the catalytic

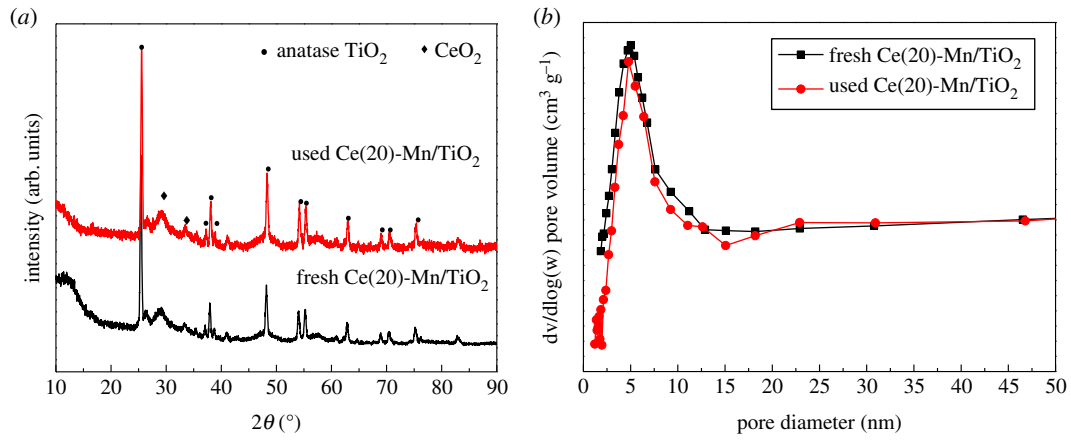


**Figure 3.** (*a*) XRD patterns and (*b*) pore size distribution of fresh and used Ce(20)-Mn/$TiO_2$ catalysts.

activity of Ce-Mn/$TiO_2$ was enhanced substantially. Catalysts were loaded with 10%, 20% and 30% Ce and denoted as Ce(10), Ce(20) and Ce(30), respectively. The temperature windows for obtaining a denitration rate higher than 90% included 160–220°C for the Ce(10)-Mn/$TiO_2$ catalyst, 140–260°C for the Ce(20)-Mn/$TiO_2$ catalyst and 160–240°C for the Ce(30)-Mn/$TiO_2$ catalyst. Therefore, the Ce(20)-Mn/$TiO_2$ catalyst had the highest NO conversion rate of 99.7% with a wide denitration low-temperature window.

In the absence of $SO_2$, all three Ce-Mn/$TiO_2$ catalysts had a NO conversion of approximately 100% (during the initial 1 h shown in figure 2*b*). After adding 100 ppm of $SO_2$, the $NH_3$–SCR activity of Ce(10)-Mn/$TiO_2$ and Ce(30)-Mn/$TiO_2$ decreased rapidly to 0% and 68% in 5 h, respectively. After $SO_2$ was removed from the stream, the Ce(10)-Mn/$TiO_2$ catalyst lost all of its activity, while the Ce(30)-Mn/$TiO_2$ catalyst only maintained an activity of approximately 65%. However, the Ce(20)-Mn/$TiO_2$ catalyst had only a small decrease of 6% in the NO conversion after 100 ppm of $SO_2$ was added in 5 h. After $SO_2$ was removed from the stream, the $NH_3$–SCR activity involving the Ce(20)-Mn/$TiO_2$ catalyst recovered completely and reached 100% NO conversion.

The effect of reaction temperature on the sulfur resistance of the Ce(20)-Mn/$TiO_2$ catalyst was investigated, and the results are shown in figure 2*c*. The addition of $SO_2$ at various reaction temperatures all had an inhibitory effect on the catalytic activity. The conversion rate of NO constantly decreased with the addition of 100 ppm $SO_2$. The decrease in catalytic activity at 140°C was the most pronounced, while the catalyst activity at 180°C had the best sulfur resistance.

The effect of the $SO_2$ concentration on the activity of the best Ce(20)-Mn/$TiO_2$ catalyst was investigated, and the results are shown in figure 2*d*. When the catalyst was at 180°C for 1 h, the addition of $SO_2$ in different concentrations decreased the catalytic activity, and there were different levels of recovery after $SO_2$ was removed from the stream. $SO_2$ had a toxic effect on the Ce(20)-Mn/$TiO_2$ catalyst, and as the concentration of $SO_2$ increased, the catalyst activity decreased. The addition of 100, 150 and 200 ppm $SO_2$ decreased the NO conversion rate from 99.7% to 94%, 90% and 83%, respectively. After removing 100 ppm of $SO_2$, the catalyst activity fully recovered; however, only partial recovery was seen after the catalyst was submitted to the higher $SO_2$ concentrations.

## 3.3. Catalyst characterization

The Ce(20)-Mn/$TiO_2$ catalyst had the best $NH_3$–SCR performance, so only fresh and used Ce(20)-Mn/$TiO_2$ catalyst were analysed for determining specific catalyst characteristics. The used catalyst was extracted after the reaction was carried out in a 100 ppm $SO_2$ atmosphere for 5 h at 180°C. The XRD patterns in figure 3*a* showed that no new peaks were observed in the used catalyst, indicating that the catalyst did not form any (or negligible) crystalline states of sulfate or the amount of the formed phase was too small in the $SO_2$ atmosphere. Based on the activity discussion mentioned above, the NO conversion rate of the Ce(20)-Mn/$TiO_2$ catalyst was approximately 94% after the addition of 100 ppm $SO_2$. Therefore, the Ce(20)-Mn/$TiO_2$ catalyst had an ideal sulfur resistance.

The specific surface area, pore volume and average pore size of the different Ce(wt%)-Mn/$TiO_2$ catalysts are summarized in table 1. Owing to the large specific surface area of $CeO_2$, the loading amount

**Table 1.** Physical properties of Ce(wt%)-Mn/$TiO_2$.

| catalyst | specific surface area ($m^2\ g^{-1}$) | pore volume ($cm^3\ g^{-1}$) | average pore size (nm) |
|---|---|---|---|
| Ce(10)-Mn/$TiO_2$ | 23.822 | 0.0575 | 11.16 |
| Ce(20)-Mn/$TiO_2$ | 35.024 | 0.0631 | 8.09 |
| Ce(30)-Mn/$TiO_2$ | 34.839 | 0.0504 | 5.06 |

**Table 2.** Physical properties of fresh and used Ce(20)-Mn/$TiO_2$ catalyst.

| catalyst | specific surface area ($m^2\ g^{-1}$) | pore volume ($cm^3\ g^{-1}$) | average pore size (nm) |
|---|---|---|---|
| fresh Ce(20)-Mn/$TiO_2$ | 35.024 | 0.0631 | 8.09 |
| used Ce(20)-Mn/$TiO_2$ | 28.092 | 0.0624 | 6.15 |

of Ce had a significant impact on the specific surface area of the catalyst. With the increase in the loading amount, the specific surface area showed a tendency to increase first and then decrease. The increase in the loading amount of Ce led to a discernable change of the specific surface area from 23.822 to 35.024 $m^2\ g^{-1}$ and finally to 34.839 $m^2\ g^{-1}$, indicating that the doping of Ce played an important role in the variation of the specific surface area of the catalyst. The surface area of Ce(10)-Mn/$TiO_2$ is relatively small, which corresponds to the lowest catalytic activity of Ce(10)-Mn/$TiO_2$ in figure 2*a*.

The specific surface area, pore volume and average pore size of the fresh and used catalyst are summarized in Table 2. The physical properties of the catalyst were impaired by $SO_2$. The addition of 100 ppm $SO_2$ decreased the respective specific surface area, pore volume and average pore size of the Ce(20)-Mn/$TiO_2$ catalyst from 35.024 $m^2\ g^{-1}$, 0.0631 $cm^3\ g^{-1}$ and 8.09 nm to 28.092 $m^2\ g^{-1}$, 0.0624 $cm^3\ g^{-1}$ and 6.15 nm, respectively. The pore size distribution of fresh and used Ce(20)-Mn/$TiO_2$ catalysts are shown in figure 3*b*. The pore structure of the fresh Ce(20)-Mn/$TiO_2$ catalyst was in the range of 2–10 nm. After the reaction, the number of pores in the range of 8–10 nm decreased slightly, while the number of pores in the 2–8 nm range did not change, ensuring there was sufficient catalytic activity. The decreased NO conversion was due to the change in the catalyst structure in terms of the pore size distribution and surface area.

The fresh and used Ce(20)-Mn/$TiO_2$ catalysts were also characterized by SEM-EDS, and the results are shown in figure 4. An agglomeration phenomenon, though not obvious, occurred on the surface of the catalyst after undergoing reactions in the $SO_2$ atmosphere (figure 4*a–b*). EDS mapping results (figure 4*c–d* and table 3) verified the existence of S and N on the surface, implying that the ammonium sulfate material formed on the surface of the used catalyst. This covered the active sites and decreased the catalytic activity. However, the XRD patterns imply that the ammonium sulfate material was not obviously detected because there is no formation or only a relatively small amount was present and therefore accounted for only a negligible decrease of the catalytic activity in the $SO_2$ atmosphere.

XPS spectra of the Ce 3d, Mn 2p and O 1s of the fresh and used Ce(20)-Mn/$TiO_2$ catalysts are shown in figure 5*a–c*. Figure 5*a* shows the Ce 3d in the fresh and used catalysts had eight peaks, where the V′, U′ were the characteristic peaks of $Ce^{3+}$ ($Ce_2O_3$), and V, V″, V‴, U, U″, U‴ were the characteristic peaks of $Ce^{4+}$. The leading form of the Ce oxide in both catalysts was $CeO_2$ ($Ce^{4+}$) which was beneficial for oxygen storage capacity. The conversion between $Ce^{3+}$ and $Ce^{4+}$ accomplished a storage-release cycle of oxygen for better promoting the process of denitration. Figure 5*b* illustrates that the peak of Mn $2p_{1/2}$ was located near 653.3 eV, while the peak of Mn $2p_{3/2}$ was composed of $Mn^{2+}$, $Mn^{3+}$ (642.0 eV) and $Mn^{4+}$ (643.0 eV). The leading form of Mn in the Ce(20)-Mn/$TiO_2$ catalyst was $Mn^{4+}$ (table 4). The catalytic effect of $MnO_x$ was related to its valence state, where $MnO_2 > Mn_2O_3 > MnO$ [22]. This has also been demonstrated by Thirupathi & Smirniotis [23]. Their group indicated that $MnO_2$ was the most active component among a series comprising $MnO_2$, $Mn_5O_8$, $Mn_2O_3$ and $Mn_3O_4$. Therefore, $Mn^{4+}$ had a superior catalytic denitration activity, and this corresponded to the best catalytic denitration activity of Ce(20)-Mn/$TiO_2$. The peaks of the Mn $2p_{1/2}$ and Mn $2p_{3/2}$ of the used catalyst shifted in the direction of a higher electron bonding energy, and the offsets were approximately 0.06 eV and 0.1 eV, respectively. This indicated that a metal sulfate formed which resulted from the sulfation of Mn [24]. The decrease of $Mn^{4+}/Mn^{3+}$ from 84.4% to 75.4% is a possible reason for the decreased $NH_3$–SCR activity. The

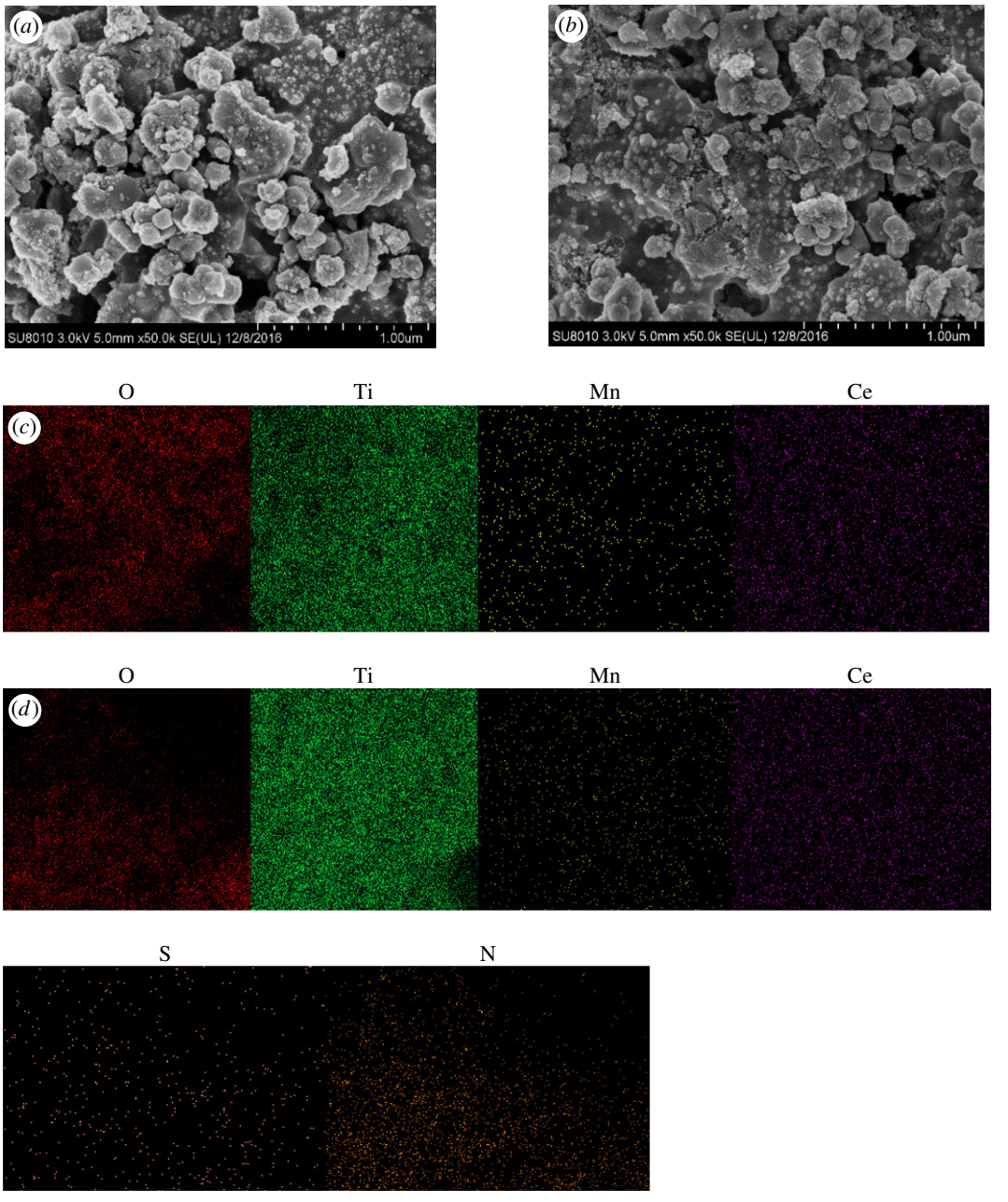


**Figure 4.** SEM micrographs of (*a*) fresh and (*b*) used Ce(20)-Mn/$TiO_2$ catalysts as well as energy dispersive spectrometer images of (*c*) fresh and (*d*) used Ce(20)-Mn/$TiO_2$ catalyst.

**Table 3.** Surface element concentration of fresh and used Ce(20)-Mn/$TiO_2$ catalyst.

| | the concentration of surface elements (%) | | | | | |
|---|---|---|---|---|---|---|
| catalyst | Ce | Mn | O | Ti | S | N |
| fresh Ce(20)-Mn/$TiO_2$ | 10.37 | 8.96 | 75.22 | 5.45 | — | — |
| used Ce(20)-Mn/$TiO_2$ | 10.1 | 8.01 | 71.41 | 5.23 | 3.28 | 1.97 |

spectrum of O 1s in figure 5*c* contains characteristic peaks of $O_\alpha$ and $O_\beta$, where $O_\beta$ belongs to the characteristic peak of lattice oxygen at a binding energy of 529.5–529.8 eV. $O_\alpha$ belongs to the surface adsorption characteristic peaks of oxygen at a binding energy of 531.8–532.5 eV [10]. In table 4, the surface adsorption of the oxygen concentration was 48.8% in the fresh catalyst, and this increased to 40.5% in the

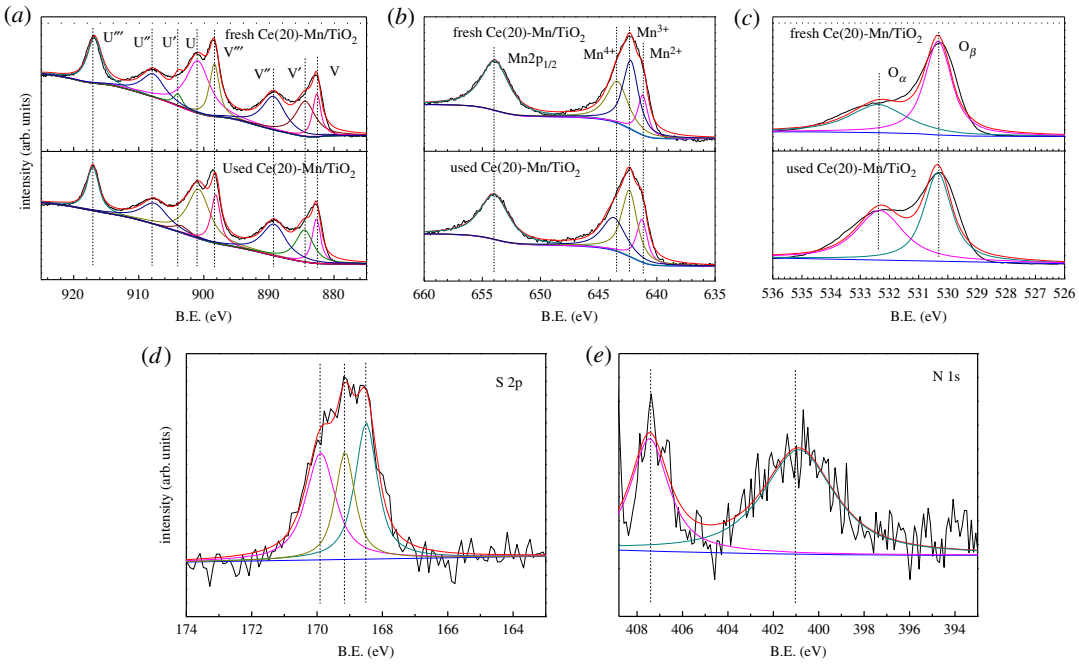


**Figure 5.** XPS spectra of fresh and used Ce(20)-Mn/$TiO_2$. (*a*) Ce 3d, (*b*) Mn 2p, (*c*) O 1s, (*d*) S 2p and (*e*) N 1s.

**Table 4.** Surface elemental valence distribution of fresh and used Ce(20)-Mn/$TiO_2$ catalyst.

| | the valence ratio of the surface elements (%) | | |
|---|---|---|---|
| catalyst | $Ce^{3+}/Ce^{4+}$ | $Mn^{4+}/Mn^{3+}$ | $O_\alpha/(O_\alpha+O_\beta)$ |
| fresh Ce (20)-Mn/$TiO_2$ | 17.5 | 84.4 | 48.8 |
| used Ce (20)-Mn/$TiO_2$ | 18.0 | 75.3 | 40.5 |

used catalyst. The high concentration of the surface adsorption of oxygen had a strong oxidation effect, which not only completed the oxidation and reduction cycle but also enhanced the oxidation process of NO to $NO_2$. This promoted a rapid response to the SCR reaction [25,26].

XPS spectra of the S 2p and N 1s of the used Ce(20)-Mn/$TiO_2$ catalysts are shown in figure 5*d–e*. Figure 5*d* shows that the leading form of S in the used catalyst was $S^{4+}$ and $S^{6+}$. The peak at 168.5 eV belonged to $SO_3^{2-}$, while the peaks at 169.9 and 169.1 eV were assigned to $SO_4^{2-}$ [24]. $S^{6+}$ accounted for approximately 63% of S and included some sulfate material which formed on the catalyst surface after undergoing reactions in the $SO_2$ atmosphere. Figure 5*e* demonstrates the peaks of N located in the vicinity of 400.8 eV and 407.3 eV were characterized as $NH_4^+$ and $NO_3^-$, respectively [27]. $NH_4^+$ accounted for approximately 64% of the total N. The conversion of $NH_3$ to $NH_4^+$ and $NO_3^-$ was indicated by the results.

# 4. Conclusion

$NH_3$–SCR activity was measured after using an IP method and a SG method to form a Ce-Mn/$TiO_2$ catalyst. The catalyst formed with the IP method had a better low-temperature denitration activity than the catalyst synthesized using the SG method. The Ce-Mn/$TiO_2$ catalyst loaded with 20% Ce had the best low-temperature activity with a NO conversion rate of 99.7% at 180°C. Despite the addition of 100 ppm $SO_2$ at 180°C for 5 h, the NO conversion rate of the Ce(20)-Mn/$TiO_2$ catalyst was still as high as 94% and recovered when $SO_2$ was removed from the stream. The $SO_2$ resistance of the Ce(20)-Mn/$TiO_2$ catalyst is attributed to the widely distributed elements of Mn and Ce. This led to the inability of the sulfate material to remain on the surface. Characterization of fresh and used Ce(20)-Mn/$TiO_2$ catalysts was performed using XRD, BET, XPS and SEM-EDS. These results indicated that there was a decrease in $Ce^{4+}$ and $Mn^{4+}$

in the used catalysts. These results also showed that the sulfate phase formation and the change of the pore structure accounted for a decrease in $NH_3$–SCR activity.

Data, accessibility. Our data are deposited at Dryad: https://doi.org/10.5061/dryad.pv12j [28].

Authors' contributions. Q.X. designed the study; W.Y. and S.C. performed the laboratory experiment; Q.X. and Y.L. analysed data; Q.X, Y.L and J.S edited the manuscript for important intellectual content; all authors wrote the manuscript and gave final approval for publication.

Competing interests. We have no competing interests.

Funding. Financial support came from National Key Research and Development Plan (No. 2016YFC0303701), Beijing Nova Program (No. Z171100001117058), Beijing Municipal Science and Technology Project (No. Z161100001316010), Science Foundation of China University of Petroleum Beijing (No. 2462018BJC004), State Key Laboratory of Petroleum and Petrochemical Pollution Control and Treatment (No. PPC2017015) and National Institute of Food and Agriculture, U.S. Department of Agriculture, and McIntire Stennis (No. 1009735)

Acknowledgements. We thank Peng Pu, Li Cao, Quangui Wu, Hongjun Zhou for their assistance with the tests. We are also grateful to two anonymous reviewers who provided comments that substantially improved the manuscript.

# References

1. Boningari T, Smirniotis PG. 2016 Impact of nitrogen oxides on the environment and human health: Mn-based materials for the $NO_x$ abatement. *Curr. Opin. Chem. Eng.* **13**, 133–141. (doi:10.1016/j.coche.2016.09.004)
2. Zhu W, Xiao S, Zhang D, Liu P, Zhou H, Dai W, Liu F, Li H. 2015 Highly efficient and stable Au/$CeO_2$-$TiO_2$ photocatalyst for nitric oxide abatement: potential application in flue gas treatment. *Langmuir* **31**, 10 822–10 830. (doi:10.1021/acs.langmuir.5b02232)
3. Liu Z, Zhu J, Li J, Ma L, Woo SI. 2014 Novel Mn–Ce–Ti mixed-oxide catalyst for the selective catalytic reduction of $NO_x$ with $NH_3$. *ACS Appl. Mater. Interfaces* **6**, 14 500–14 508. (doi:10.1021/am5038164)
4. Yan L, Guda VK, Hassan E, Steele PH, Mitchell B, Fei Y. 2016 Hydrodeoxygenation of oxidized distilled bio-oil for the production of gasoline fuel type. *Energy Convers. Manage.* **112**, 319–327. (doi:10.1016/j.enconman.2015.12.047)
5. Luo Y, Guda VK, Steele PH, Wan H. 2016 Hydrodeoxygenation of oxidized and hydrotreated bio-oils to hydrocarbons in fixed-bed continuous reactor. *BioResources* **11**, 4415–4431. (doi:10.15376/biores.11.2.4415-4431)
6. Lu X, Fung JCH, Wu D. 2015 Modeling wet deposition of acid substances over the PRD region in China. *Atmos. Environ.* **122**, 819–828. (doi:10.1016/j.atmosenv.2015.09.035)
7. Radojevic M. 1998 Reduction of nitrogen oxides in flue gases. *Environ. Pollut.* **102**, 685–689. (doi:10.1016/S0269-7491(98)80099-7)
8. Busca G, Lietti L, Ramis G, Berti F. 1998 Chemical and mechanistic aspects of the selective catalytic reduction of $NO_x$ by ammonia over oxide catalysts: a review. *Appl. Catal. B* **18**, 1–36. (doi:10.1016/s0926-3373(98)00040-x)
9. Yan L, Liu Y, Zha K, Li H, Shi L, Zhang D. 2017 Scale–activity relationship of $MnO_x$-$FeO_y$ nanocage catalysts derived from Prussian blue analogues for low-temperature NO reduction: experimental and DFT studies. *ACS Appl. Mater. Interfaces* **9**, 2581–2593. (doi:10.1021/acsami.6b15527)
10. Li Y, Wan Y, Li Y, Zhan S, Guan Q, Tian Y. 2016 Low-temperature selective catalytic reduction of NO with $NH_3$ over $Mn_2O_3$-doped $Fe_2O_3$ hexagonal microsheets. *ACS Appl. Mater. Interfaces* **8**, 5224–5233. (doi:10.1021/acsami.5b10264)
11. Huang HY, Yang RT. 2001 Removal of NO by reversible adsorption on Fe–Mn based transition metal oxides. *Langmuir* **17**, 4997–5003. (doi:10.1021/la0102657)
12. Chen L, Si Z, Wu X, Weng D. 2014 DRIFT study of CuO–$CeO_2$–$TiO_2$ mixed oxides for $NO_x$ reduction with $NH_3$ at low temperatures. *ACS Appl. Mater. Interfaces* **6**, 8134–8145. (doi:10.1021/am5004969)
13. Cheng K, Liu J, Zhang T, Li J, Zhao Z, Wei Y, Jiang G, Duan A. 2014 Effect of Ce doping of $TiO_2$ support on $NH_3$-SCR activity over $V_2O_5$–$WO_3$/$CeO_2$–$TiO_2$ catalyst. *J. Environ. Sci.* **26**, 2106–2113. (doi:10.1016/j.jes.2014.08.010)
14. Ding S, Liu F, Shi X, Liu K, Lian Z, Xie L, He H. 2015 Significant promotion effect of Mo additive on a novel Ce–Zr mixed oxide catalyst for the selective catalytic reduction of $NO_x$ with $NH_3$. *ACS Appl. Mater. Interfaces* **7**, 9497–9506. (doi:10.1021/acsami.5b00636)
15. Xu Q, Zhao J, Xu H, Zhou H. 2015 Dispersion of $TiO_2$ particles and preparation of $SiO_2$ coating layers on the surfaces of $TiO_2$. *Mater. Res. Innov.* **19**, S5-142–S145-145. (doi:10.1179/1432891715Z)
16. Shi X, Xu Q, Tian A, Tian Y, Xue X, Sun H, Yang H, Dong C. 2015 Antibacterial activities of $TiO_2$ nanotubes on *Porphyromonas gingivalis*. *RSC Adv.* **5**, 34 237–34 242. (doi:10.1039/C5RA00804B)
17. Cen Y, Yao Y, Xu Q, Xia Z, Sisson RD, Liang J. 2016 Fabrication of $TiO_2$–graphene composite for the enhanced performance of lithium batteries. *RSC Adv.* **6**, 66 971–66 977. (doi:10.1039/c6ra08144d)
18. Qi G, Yang RT, Chang R. 2004 $MnO_x$-$CeO_2$ mixed oxides prepared by co-precipitation for selective catalytic reduction of NO with $NH_3$ at low temperatures. *Appl. Catal. B* **51**, 93–106. (doi:10.1016/j.apcatb.2004.01.023)
19. Lee SM, Park KH, Hong SC. 2012 $MnO_x$/$CeO_2$–$TiO_2$ mixed oxide catalysts for the selective catalytic reduction of NO with $NH_3$ at low temperature. *Chem. Eng. J.* **195**, 323–331. (doi:10.1016/j.cej.2012.05.009)
20. Cheng X, Bi XT. 2014 A review of recent advances in selective catalytic $NO_x$ reduction reactor technologies. *Particuology* **16**, 1–18. (doi:10.1016/j.partic.2014.01.006)
21. Liu J *et al.* 2012 Potassium-modified molybdenum-containing SBA-15 catalysts for highly efficient production of acetaldehyde and ethylene by the selective oxidation of ethane. *J. Catal.* **285**, 134–144. (doi:10.1016/j.jcat.2011.09.029)
22. Kapteijn F, Singoredjo L, Andreini A, Moulijn J. 1994 Activity and selectivity of pure manganese oxides in the selective catalytic reduction of nitric oxide with ammonia. *Appl. Catal. B* **3**, 173–189. (doi:10.1016/0926-3373(93)e0034-9)
23. Thirupathi B, Smirniotis PG. 2012 Nickel-doped Mn/$TiO_2$ as an efficient catalyst for the low-temperature SCR of NO with $NH_3$: Catalytic evaluation and characterizations. *J. Catal.* **288**, 74–83. (doi:10.1016/j.jcat.2012.01.003)
24. Romano EJ, Schulz KH. 2005 A XPS investigation of $SO_2$ adsorption on ceria–zirconia mixed-metal oxides. *Appl. Surf. Sci.* **246**, 262–270. (doi:10.1016/j.apsusc.2004.11.017)
25. Wu Z, Jin R, Wang H, Liu Y. 2009 Effect of ceria doping on $SO_2$ resistance of Mn/$TiO_2$ for selective catalytic reduction of NO with $NH_3$ at low temperature. *Catal. Commun.* **10**, 935–939. (doi:10.1016/j.catcom.2008.12.032)
26. Qi G, Li W. 2015 NO oxidation to $NO_2$ over manganese-cerium mixed oxides. *Catal. Today* **258**, 205–213. (doi:10.1016/j.cattod.2015.03.020)
27. Bohao C, Yunsheng M, Liangbing D, Lingshun X, Zongfang W, Qing Y, HUANG W. 2013 XPS and TPD study of NO interaction with Cu (111): role of different oxygen species. *Chin. J. Catal.* **34**, 964–972. (doi:10.1016/s1872-2067(12)60585-3)
28. Xu Q, Yang W, Cui S, Street J, Luo Y. 2018 Data from: Sulfur resistance of Ce-Mn/$TiO_2$ catalysts for Low-temperature $NH_3$–SCR. Dryad Digital Repository. (doi:10.5061/dryad.pv12j)